PROCEEDINGS OF SCIENCE

Measurement of fragmentation functions and angular and momentum distributions of charged particles within and around jets in Pb+Pb and pp collisions at $\sqrt{s_{\rm NN}} = 5.02$ TeV with ATLAS at the LHC

Akshat Puri* **for the ATLAS Collaboration**
University of Illinois at Urbana-Champaign, IL 61820, USA
E-mail: apuri@cern.ch

Studies of the fragmentation of jets into charged particles in heavy-ion collisions can help in understanding the mechanism of jet quenching by the hot and dense QCD matter created in such collisions, the quark-gluon plasma. These proceedings present measurements of the fragmentation functions of inclusive jets, the angular distribution of charged particles in and around such jets, and the fragmentation functions of photon-tagged jets, in $\sqrt{s_{\rm NN}} = 5.02$ TeV Pb+Pb and pp collisions, done using the ATLAS detector at the LHC. The measurements are performed for jets reconstructed with the anti-k_t algorithm with radius parameter $R = 0.4$.

International Conference on Hard and Electromagnetic Probes of High-Energy Nuclear Collisions
October 4th, 2018
Aix-Les-Bains, Savoie, France

*Speaker.

PoS(HardProbes2018)002

1. Introduction

Ultra-relativistic nuclear collisions at the Large Hadron Collider (LHC) produce hot, dense matter called the quark-gluon plasma, QGP [1, 2]. Hard-scattering processes in these collisions produce jets that interact with the QGP, and the comparison of the rates and the characteristics of these jets in heavy-ion and pp collisions provides information on its properties.

These proceedings present three complimentary measurements of the inclusive jet fragmentation functions [3], the fragmentation functions for photon-tagged jets [4], and the angular distribution of charged particles in and around inclusive jets [5]. Previous measurements of the transverse jet profile [6] and the longitudinal fragmentation function [3,7–9] showed an excess of both low and high momentum particles inside the jet compared to pp collisions, suggesting that the energy lost by jets through the jet-quenching process is being transferred to soft particles within and around the jet [10, 11]. Measurements of the yields of these particles as a function of their transverse momentum, as well as the distance from the jet axis have the potential to constrain the models of jet energy loss processes in Pb+Pb collisions. The inclusive jet fragmentation function measurement differs from the photon-tagged jet fragmentation function measurement in that the latter is done to lower $p_{\mathrm{T}}^{\mathrm{jet}}$, and probes a different ratio of quark to gluon jets. Additionally, the inclusive jet measurement selects on jets that are already quenched, while the photon-tagged measurement uses photons unaffected by the quark gluon plasma.

The fragmentation functions are measured as a function of the charged-particle transverse momentum p_{T}, and the charged-particle longitudinal momentum fraction with respect to the jet, $z \equiv p_{\mathrm{T}} \cos \Delta R / p_{\mathrm{T}}^{\mathrm{jet}}$, where $\Delta R = \sqrt{\Delta\eta^2 + \Delta\phi^2}$ is the distance between the jet axis and the charged-particle direction[1]. These observables are sensitive to the properties of the medium, and can be expressed as

$$D(p_{\mathrm{T}}) = \frac{1}{N_{\mathrm{jet}}} \frac{\mathrm{d}n_{\mathrm{ch}}}{\mathrm{d}p_{\mathrm{T}}}, \quad D(z) \quad = \frac{1}{N_{\mathrm{jet}}} \frac{\mathrm{d}n_{\mathrm{ch}}}{\mathrm{d}z} \tag{1.1}$$

The angular distribution of charged particles as a function of the distance from the jet cone is given by

$$D(p_{\mathrm{T}}, r) = \frac{1}{N_{\mathrm{jet}}} \frac{1}{2\pi r} \frac{\mathrm{d}^2 n_{\mathrm{ch}}(r)}{\mathrm{d}r \mathrm{d}p_{\mathrm{T}}} \tag{1.2}$$

Here N_{jet} is the total number of jets; n_{ch} is the number of charged particles; $2\pi r$ is the circumference of the annulus at a given distance r from the jet axis, and dr is the width of the annulus.

The ratios of the distributions measured in Pb+Pb and pp collisions allows quantifying the modification in yields from the pp to the Pb+Pb system.

$$R_{D(p_{\mathrm{T}})} = \frac{D(p_{\mathrm{T}})_{\mathrm{Pb+Pb}}}{D(p_{\mathrm{T}})_{pp}}, \quad R_{D(z)} = \frac{D(z)_{\mathrm{Pb+Pb}}}{D(z)_{pp}}, \quad R_{D(p_{\mathrm{T}},r)} = \frac{D(p_{\mathrm{T}},r)_{\mathrm{Pb+Pb}}}{D(p_{\mathrm{T}},r)_{pp}} \tag{1.3}$$

[1] ATLAS uses a right-handed coordinate system with its origin at the nominal interaction point (IP) in the center of the detector, and the z-axis along the beam pipe. The x-axis points from the IP to the center of the LHC ring, and the y-axis points upward. Cylindrical coordinates (r, ϕ) are used the transverse plane, ϕ being the azimuthal angle around the z-axis. The pseudorapidity is defined in terms of the polar angle θ as $\eta = -\ln\tan(\theta/2)$. $\Delta R = \sqrt{(\Delta\eta)^2 + (\Delta\phi)^2}$ gives the angular distance between two objects with relative differences $\Delta\eta$ and $\Delta\phi$ in pseudorapidity and azimuth respectively.

PoS(HardProbes2018)002

2. Datasets

The measurements described in these proceedings use 25 pb^{-1} of $\sqrt{s}$ = 5.02 TeV pp data and 0.49 nb^{-1} of $\sqrt{s_{\mathrm{NN}}}$ = 5.02 TeV Pb+Pb data collected in 2015. The data were recorded using the ATLAS calorimeter, inner detector, trigger, and data acquisition systems [12].

The performance of the detector and analysis procedure was evaluated using 1.8 $\times 10^7$ simulated 5.02 TeV POWHEG+PYTHIA8 [13, 14] pp hard-scattering events, generated using the A14 tune [15] and the NNPDF23LO PDF set [16], for pp and 1.8 $\times 10^7$ 5.02 TeV hard-scattering dijet events generated with POWHEG+PYTHIA8 overlaid on top of events from the enhanced minimum-bias Pb+Pb data sample for Pb+Pb. In both samples, the detector response is simulated using GEANT4 [17, 18].

In Pb+Pb collisions, the event centrality reflects the overlap area of the two colliding nuclei and is characterized by $\Sigma E_{\mathrm{T}}^{\mathrm{FCal}}$, the total transverse energy deposited in the FCal [19]. The six centrality intervals used in these analyses are defined according to successive percentiles of the $\Sigma E_{\mathrm{T}}^{\mathrm{FCal}}$ distribution obtained in minimum-bias collisions, ordered from the most central (highest $\Sigma E_{\mathrm{T}}^{\mathrm{FCal}}$) to the most peripheral (lowest $\Sigma E_{\mathrm{T}}^{\mathrm{FCal}}$) collisions: 0–10%, 10–20%, 20–30%, 30–40%, 40–60%, 60–80%. A weight is assigned to each MC event such that the event sample obtained from the simulation has the same $\Sigma E_{\mathrm{T}}^{\mathrm{FCal}}$ distribution as in data.

Further details on the datasets used for the inclusive jet fragmentation functions, photon-tagged fragmentation functions, and the angular charged-particle distribution can be found in [3], [4], and [5] respectively.

3. Data Analysis

The jets used in all three analyses are reconstructed using the anti-k_t algorithm, run on calorimetric towers of size $\Delta\eta \times \Delta\phi = 0.1 \times 0.1$, with the radius parameter set to $R = 0.4$ [20]. Photon reconstruction uses a procedure described in [21], and is based on energy clusters in the electromagnetic calorimeter. Photon identification is done based on shapes of the electromagnetic shower in the calorimeter [22], selecting those clusters that are compatible with single photon shower patterns.

Reconstructed tracks are associated with a reconstructed jet and are corrected for a variety of effects including tracking efficiency, underlying event (UE), fakes, bin migration due to jet energy and track momentum resolution, as well as effects from the finite jet and track angular resolutions. Full details on the analyses procedure for these measurements can be seen in [3–5].

All three measurements incorporate a two-dimensional Bayesian unfolding procedure [23] as implemented in the RooUnfold package [24], to remove the effects of the bin migration due to the jet energy and track-momentum resolution. This is done because the calorimetric jet energy response depends on the fragmentation pattern of the jet [25]. Using the MC samples, four-dimensional response matrices are created using the generator-level and reconstructed $p_{\mathrm{T}}^{\mathrm{jet}}$, and the generator-level and reconstructed charged-particle $p_{\mathrm{T}}^{\mathrm{ch}}$. Separate unfolding matrices are constructed for pp data and each centrality in Pb+Pb collisions. A separate one-dimensional Bayesian unfolding is applied to correct the measured $p_{\mathrm{T}}^{\mathrm{jet}}$ spectra that are used in the normalization of the fragmentation functions and the angular distributions. The entire procedure allows for direct comparison not only between the three measurements, but also to theory predictions.

The performance of the full analysis procedure is validated in MC events where the entire correction procedure is performed using reconstructed jets and tracks, and the results are compared to the generator-level distributions. These deviations in this comparison are included in the systematic uncertainties.

4. Results

This section presents the fragmentation function measurements for both inclusive and photon-tagged jets, as well as the charged-particle angular distributions in and around inclusive jets. The modifications between the Pb+Pb and pp systems are also shown.

Figure 1 shows the $D(p_{\mathrm{T}})$, $R_{D(p_{\mathrm{T}})}$, and $R_{D(z)}$distributions for inclusive jets, as well as their dependence on the collision energy and the $p_{\mathrm{T}}^{\mathrm{jet}}$ [3]. It can be seen from Fig. 1b that there is an enhancement of particle yields at low and hight p_{T}, with a reduction of intermediate p_{T} particles. Furthermore, this modification is quantitatively consistent with that at $\sqrt{s_{\mathrm{NN}}}$= 2.76 TeV [7–9]. Figure 1c suggests that the soft particle excess in central Pb+Pb collisions exhibits a much smaller $p_{\mathrm{T}}^{\mathrm{jet}}$ dependence for the $D(p_{\mathrm{T}})$ ratios than for the $D(z)$ ratios. No $p_{\mathrm{T}}^{\mathrm{jet}}$ dependence is observed at high z for jets with $p_{\mathrm{T}}^{\mathrm{jet}}$ < 400 GeV, as seen in Fig. 1d. The $p_{\mathrm{T}}^{\mathrm{jet}}$ dependence shows scaling with z for hard fragments and scaling with p_{T} for soft fragments; this could suggest that the excess of high z particles is related to the fragmentation mechanism, and the excess of soft particles is governed by effects from the QGP [3].

Figure 2 shows the $D(p_{\mathrm{T}})$ and $R_{D(p_{\mathrm{T}})}$ distributions for photon-tagged jets [4]. It can be seen from Fig. 2a that photon-tagged jets in pp collisions have more high p_{T} particles in the final state than inclusive jets. This is consistent with observations in [26–28], that quark jets fragment harder than gluon jets, since the photon-tagged jets have a higher quark fraction than inclusive jets. Fig. 2b shows that the minimum in the $R_{D(p_{\mathrm{T}})}$ ratio for photon-tagged jets in central Pb+Pb is shifted to larger p_{T} as the centrality increases, with the high p_{T} region giving a ratio consistent with unity. These modifications (in central Pb+Pb) are larger than those in inclusive jets, with an additional relative suppression at high p_{T}, and a counter-balancing enhancement at low p_{T}. For 30-80% Pb+Pb, the $R_{D(p_{\mathrm{T}})}$ distribution for both inclusive and photon-tagged jets is qualitatively similar.

Figure 3 shows the angular distribution of charged particles as a function of r in pp and Pb+Pb collisions, as well as the modification from the pp to the Pb+Pb system [5]. A broadening (narrowing) of the $D(p_{\mathrm{T}},r)$ distribution for $p_{\mathrm{T}} < 4$ GeV ($p_{\mathrm{T}} > 4$ GeV) particles inside the jet in central Pb+Pb collisions compared to pp collisions is observed. Figure 3b shows that the modification to the angular distribution in Pb+Pb is above (below) unity at all r for charged particles with $p_{\mathrm{T}} < 4$ GeV ($p_{\mathrm{T}} > 4$ GeV), and increases (decreases) for $r < 0.3$, being approximately constant thereafter. The $p_{\mathrm{T}}^{\mathrm{jet}}$ dependence to the $R_{D(p_{\mathrm{T}},r)}$ distributions can be seen in Fig. 3c, where low p_{T} (1.6 - 2.5 GeV) particles show a $p_{\mathrm{T}}^{\mathrm{jet}}$ dependent enhancement between $0.1 < r < 0.25$. No significant $p_{\mathrm{T}}^{\mathrm{jet}}$ dependence is observed for high p_{T} (6.3 - 10.0 GeV) particles. The size of the modifications in Pb+Pb compared to pp monotonically depends on the collision centrality, and can be seen in Fig. 3d.

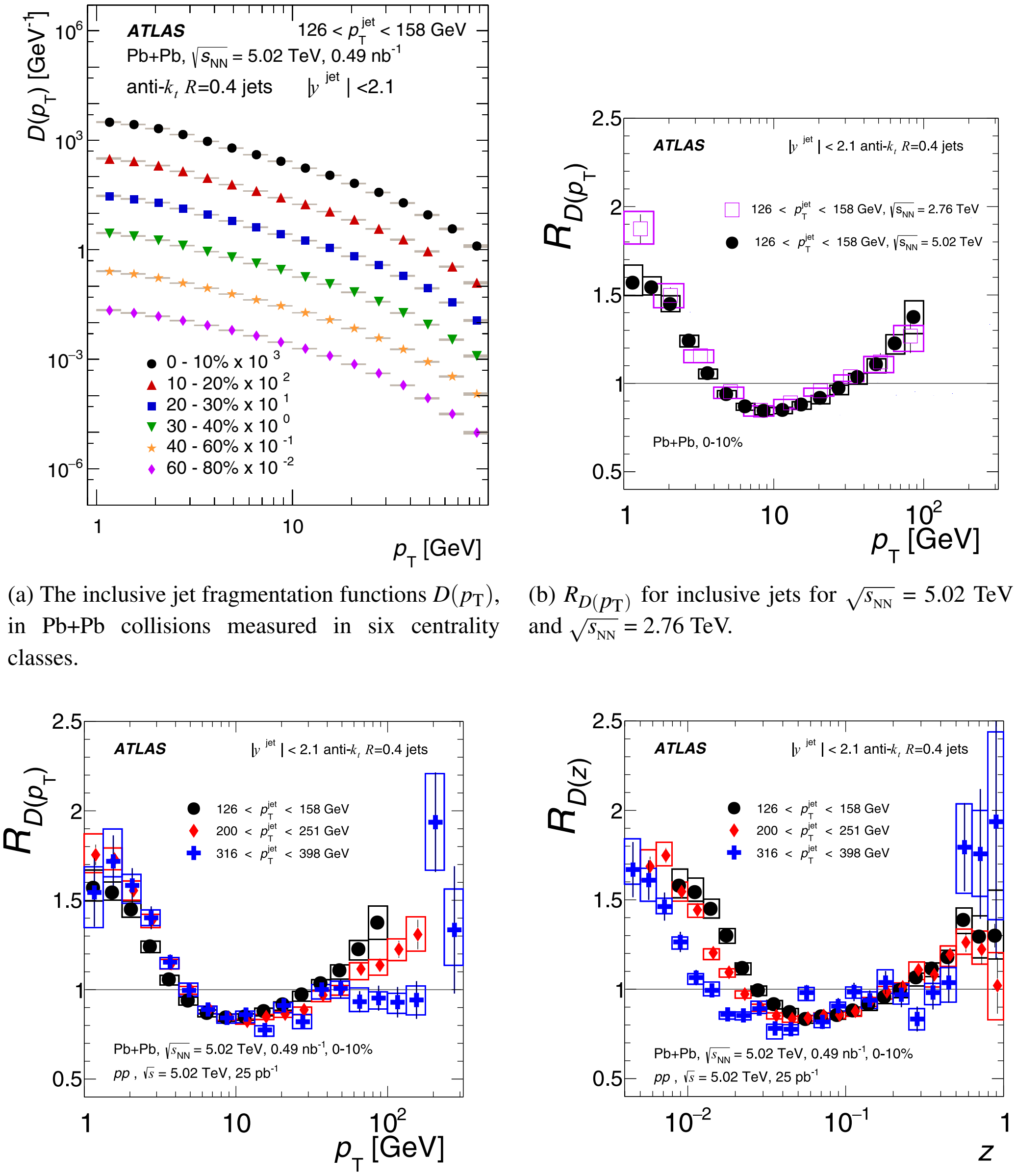

(a) The inclusive jet fragmentation functions $D(p_T)$, in Pb+Pb collisions measured in six centrality classes.

(b) $R_{D(p_T)}$ for inclusive jets for $\sqrt{s_{NN}}$ = 5.02 TeV and $\sqrt{s_{NN}}$ = 2.76 TeV.

(c) The p_T^{jet} dependence to the $R_{D(p_T)}$ distributions.

(d) The p_T^{jet} dependence to the $R_{D(z)}$ distributions.

Figure 1: Inclusive jet fragmentation function measurements. The vertical bars (shaded bands) indicate statistical (systematic) uncertainties. Figures are from [3].

5. Conclusions

These proceedings present a measurement of the fragmentation functions for inclusive and photon-tagged jets, as well as the angular distribution of charged particles around the jet axis.

Centrality dependence modifications to the inclusive jet fragmentation functions are observed in Pb+Pb collisions when compared to those in pp collisions, with the magnitude of the modification increasing with increasing collisions centrality. A comparison of the modifications of the

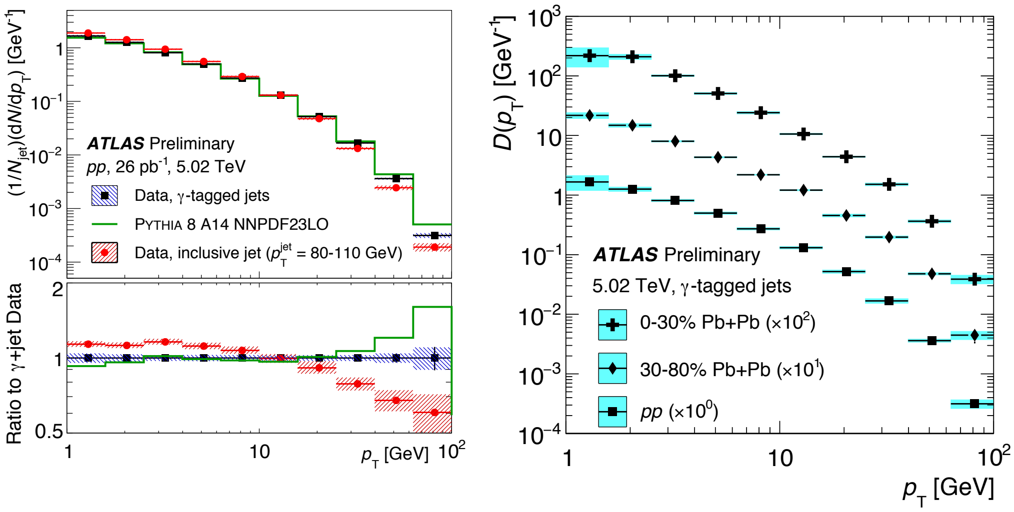

(a) The photon-tagged jet fragmentation functions $D(p_\mathrm{T})$ in pp data (black) and PYTHIA 8 MC (green) and Pb+Pb collisions. The $D(p_\mathrm{T})$ distributions for inclusive jets in data (red) are also shown.

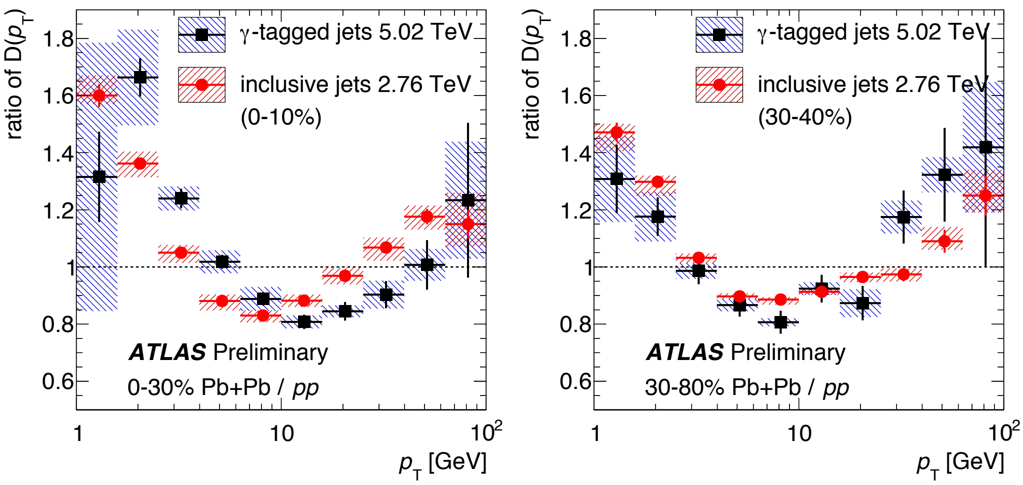

(b) The $R_{D(p_\mathrm{T})}$ distributions for inclusive and photon-tagged jets for central and peripheral collisions.

Figure 2: Photon-tagged jet fragmentation function measurements. The vertical bars (shaded bands) indicate statistical (systematic) uncertainties. Figures are from [4].

inclusive jet fragmentation functions as a function of $p_\mathrm{T}^\mathrm{jet}$ shows whether the size of modifications scales with charged-particle z (indicating fragmentation effects) or with p_T (indicating a medium effect). The photon tagging of jets explores the dependence of the fragmentation on the flavor composition, with these jets having a higher quark to gluon fraction than inclusive jets. Photon-tagged jets in central collisions also show greater modifications than compared to inclusive jets. Since the p_T dependence of the fragmentation function modification [3] suggest that the flavor-dependence is small, the differences may arise from a bias in the initial selection of the jets based on $p_\mathrm{T}^\mathrm{jet}$ [4]. The modifications in the angular distribution of charged particles within and around jets suggest that the energy lost by jets, through the jet quenching process, is being transferred to particles with

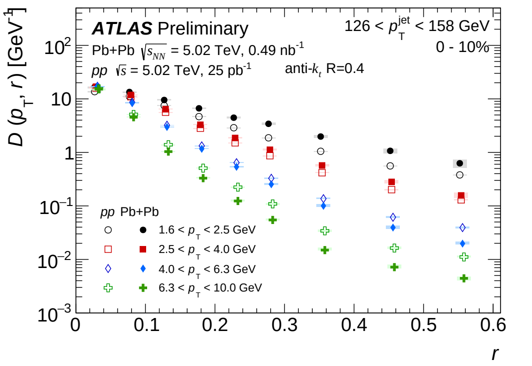

(a) The angular distributions of charged particles as a function of distance from the jet axis for four p_T selections in 0-10% Pb+Pb (closed) and pp (open) collisions.

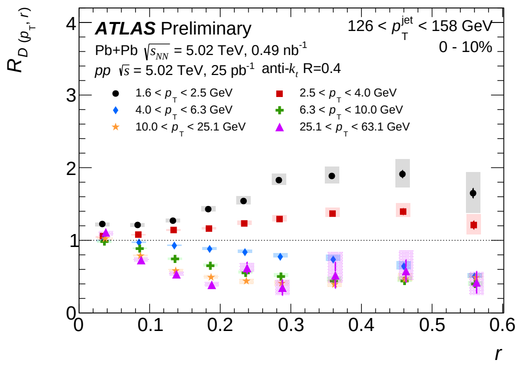

(b) The $R_{D(p_T,r)}$distributions as a function of distance from the jet axis, for different p_T ranges, in 0-10% Pb+Pb collisions.

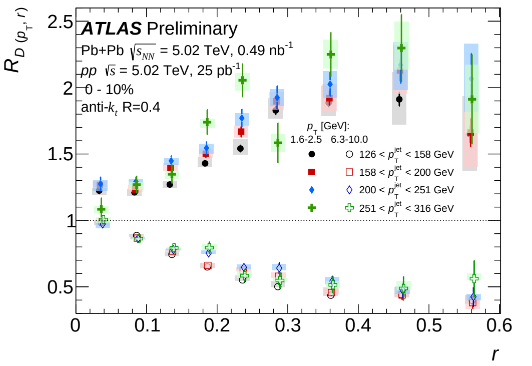

(c) The $R_{D(p_T,r)}$ distributions as a function of distance from the jet axis for low and high p_T particles, for different p_T^{jet} ranges, in 0-10% Pb+Pb collisions.

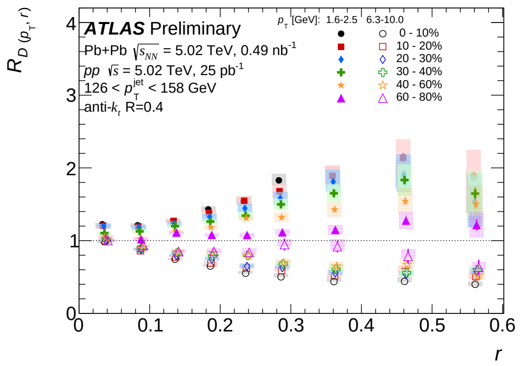

(d) The $R_{D(p_T,r)}$ distributions as a function of distance from the jet axis for low and high p_T particles, for different Pb+Pb collision centrality classes.

Figure 3: Measurements of the angular distribution of charged particles. The vertical bars (shaded bands) indicate statistical (systematic) uncertainties. Figures are from [5].

$p_T < 4.0$ GeV at larger radial distances. This is qualitatively consistent with theoretical calculations [10, 11, 29–33]. These ATLAS measurements, along with other measurements of the jet R_{AA} [34] and dijet asymmetry [35], are essential to constraining the physics of jet quenching.

References

[1] G. Roland, K. Šafařík, and P. Steinberg. Heavy-ion collisions at the LHC. *Prog. Part. Nucl. Phys.*, 77:70–127, 2014.

[2] Wit Busza et al. Heavy Ion Collisions: The Big Picture, and the Big Questions. *Ann. Rev. Nucl. Part. Sci.*, 68:339–376, 2018.

[3] ATLAS Collaboration. Measurement of jet fragmentation in Pb+Pb and pp collisions at $\sqrt{s_{NN}} = 5.02$ tev with the ATLAS detector. *Phys. Rev. C*, 98:024908, Aug 2018.

[4] ATLAS Collaboration. Measurement of the fragmentation function for photon-tagged jets in $\sqrt{s_{\mathrm{NN}}} = 5.02$ TeV Pb+Pb and pp collisions with the ATLAS detector. (ATLAS-CONF-2017-074), CERN, Geneva, Sep 2017.

[5] ATLAS Collaboration. Measurement of angular and momentum distributions of charged-particles within and around jets in Pb+Pb and pp collisions at $\sqrt{s_{NN}} = 5.02$ TeV with ATLAS at the LHC. (ATLAS-CONF-2018-010), CERN, Geneva, May 2018.

[6] CMS Collaboration. Modification of jet shapes in PbPb collisions at $\sqrt{s_{NN}} = 2.76$ TeV. *Phys. Lett.*, B730:243–263, 2014.

[7] ATLAS Collaboration. Measurement of inclusive jet charged-particle fragmentation functions in Pb+Pb collisions at $\sqrt{s_{NN}} = 2.76$ TeV with the ATLAS detector. *Phys. Lett. B*, 739:320–342, 2014.

[8] CMS Collaboration. Measurement of jet fragmentation in PbPb and pp collisions at $\sqrt{s_{NN}} = 2.76$ TeV. *Phys. Rev. C*, 90:024908, 2014.

[9] ATLAS Collaboration. Measurement of jet fragmentation in Pb+Pb and pp collisions at $\sqrt{s_{\mathrm{NN}}} = 2.76$ TeV with the ATLAS detector at the LHC. *Eur. Phys. J. C*, 77(6):379, 2017.

[10] Guang-You Qin and Xin-Nian Wang. Jet quenching in high-energy heavy-ion collisions. *Int. J. Mod. Phys. E*, 24(11):1530014, 2015.

[11] Jean-Paul Blaizot et al. Angular structure of the in-medium QCD cascade. *Phys. Rev. Lett.*, 114(22):222002, 2015.

[12] ATLAS Collaboration. The ATLAS Experiment at the CERN Large Hadron Collider. *JINST*, 3:S08003, 2008.

[13] Paolo Nason. A New method for combining NLO QCD with shower Monte Carlo algorithms. *JHEP*, 11:040, 2004.

[14] Torbjörn Sjöstrand et al. An Introduction to PYTHIA 8.2. *Comput. Phys. Commun.*, 191:159–177, 2015.

[15] ATLAS Collaboration. ATLAS Run 1 Pythia8 tunes. (ATL-PHYS-PUB-2014-021), CERN, Geneva, Nov 2014.

[16] Richard D. Ball et al. Parton distributions with LHC data. *Nucl. Phys. B*, 867:244–289, 2013.

[17] GEANT4 Collaboration, S. Agostinelli et al. GEANT4: A simulation toolkit. *Nucl. Instrum. Meth. A*, 506:250–303, 2003.

[18] ATLAS Collaboration. The ATLAS Simulation Infrastructure. *Eur. Phys. J.*, C70:823–874, 2010.

[19] ATLAS Collaboration. Measurement of longitudinal flow de-correlations in Pb+Pb collisions at $\sqrt{s_{\mathrm{NN}}} = 2.76$ and 5.02 TeV with the ATLAS detector. *Eur. Phys. J. C*, 78(2):142, 2018.

PoS(HardProbes2018)002

[20] Matteo Cacciari, Gavin P. Salam, and Gregory Soyez. The Anti-k(t) jet clustering algorithm. *JHEP*, 0804:063, 2008.

[21] ATLAS Collaboration. Centrality, rapidity, and transverse momentum dependence of isolated prompt photon production in lead-lead collisions at $\sqrt{s_{NN}} = 2.76$ tev measured with the atlas detector. *Phys. Rev. C*, 93:034914, Mar 2016.

[22] Morad Aaboud et al. Measurement of the photon identification efficiencies with the ATLAS detector using LHC Run-1 data. *Eur. Phys. J.*, C76(12):666, 2016.

[23] G. D'Agostini. A Multidimensional unfolding method based on Bayes' theorem. *Nucl. Instrum. Meth. A*, 362:487–498, 1995.

[24] Tim Adye. Unfolding algorithms and tests using RooUnfold. *Proceedings of the PHYSTAT 2009 Workshop, CERN, Geneva, Switzerland, CERN-2011-006, pp 313*, 2011.

[25] ATLAS Collaboration. Jet energy measurement with the ATLAS detector in proton-proton collisions at $\sqrt{s} = 7$ TeV. *Eur. Phys. J. C*, 73:2304, 2013.

[26] OPAL Collaboration. Experimental properties of gluon and quark jets from a point source. *Eur. Phys. J. C*, 11:217–238, 1999.

[27] ALEPH Collaboration and R. Barate et al. Measurements of the structure of quark and gluon jets in hadronic z decays. *The European Physical Journal C - Particles and Fields*, 17(1):1–18, Oct 2000.

[28] OPAL Collaboration. A Model independent measurement of quark and gluon jet properties and differences. *Z. Phys.*, C68:179–202, 1995.

[29] Jorge Casalderrey-Solana et al. Angular Structure of Jet Quenching Within a Hybrid Strong/Weak Coupling Model. *JHEP*, 03:135, 2017.

[30] Zachary Hulcher et al. Resolution effects in the hybrid strong/weak coupling model. *Journal of High Energy Physics*, 2018(3):10, Mar 2018.

[31] Yang-Ting Chien et al. Jet Quenching from QCD Evolution. *Phys. Rev.*, D93(7):074030, 2016.

[32] Zhong-Bo Kang et al. Inclusive production of small radius jets in heavy-ion collisions. *Phys. Lett.*, B769:242–248, 2017.

[33] Martin Spousta and Brian Cole. Interpreting single jet measurements in Pb + Pb collisions at the LHC. *Eur. Phys. J. C*, 76(2):50, 2016.

[34] ATLAS Collaboration. Measurements of the Nuclear Modification Factor for Jets in Pb+Pb Collisions at $\sqrt{s_{\mathrm{NN}}} = 2.76$ TeV with the ATLAS Detector. *Phys. Rev. Lett.*, 114:072302, 2015.

[35] ATLAS Collaboration. Observation of a Centrality-Dependent Dijet Asymmetry in Lead-Lead Collisions at $\sqrt{s_{NN}} = 2.76$ TeV with the ATLAS Detector at the LHC. *Phys. Rev. Lett.*, 105:252303, 2010.